Acta Geotechnica (2017) 12:441–451
DOI 10.1007/s11440-016-0478-0

RESEARCH PAPER

Influence of physico-chemical components on the consolidation behavior of soft kaolinites

Sudhakar Rao[1] · G. B. Deepak[1] · P. Raghuveer Rao[1] · P. Anbazhagan[1]

Received: 23 October 2015 / Accepted: 29 June 2016 / Published online: 19 July 2016

Abstract Pore solution salinity has important bearing on engineering behavior of marine sediments as they influence electrochemical stress (A–R) and differential osmotic stress ($\Delta\pi$) of the salt-enriched clays. The electrochemical stress (A–R) is contributed by van der Waals (A) attraction and diffuse ion layer repulsion (R), while the differential osmotic stress ($\Delta\pi$) is governed by the differences in dissolved salt concentrations in solutions separated by osmotic membrane. The paper examines the relative influence of differential osmotic stress ($\Delta\pi$) and electrochemical stress (A–R) on the consolidation behavior of slurry consolidated kaolinite specimens, which are known to be encountered in recent alluvial marine sediments. Methods are described to evaluate the magnitudes of these physico-chemical components and their incorporation in true effective stress. Results of the study demonstrate that differential osmotic stress finitely contributes to true effective stress. The contribution from differential osmotic stress enables kaolinite specimens to sustain larger void ratio during consolidation.

Keywords Chemical forces · Clays · Consolidation · Osmotic suction

1 Introduction

Studies on low activity clay minerals, such as kaolinites, are important as they occur in recent alluvial marine sediments that are subject to alterations in pore solution salinity from sea water intrusion or fresh water flow [1, 10, 12, 14, 18, 19, 22, 26, 28, 29, 35, 41]. Alterations in pore water salinity and associated ion exchange reactions influence electrochemical stress (A–R) and differential osmotic stress ($\Delta\pi$) of clay–water suspensions [9, 13, 30, 33]; differential osmotic stress ($\Delta\pi$) arise from differences in dissolved salt concentration in pore water and external reservoir and is calculated as:

$$\Delta\pi = (M_1 - M_2) \times R'T \quad (1)$$

where R′ is universal gas constant (8.32 l kPa/mol K), T is absolute temperature (degree Kelvin), and M_1 and M_2 are dissolved salt concentrations in pore water (M_1) and consolidometer reservoir water (M_2), respectively. The electrochemical stress (A–R) is contributed by van der Waals (A) attraction and diffuse ion layer repulsion (R) [9, 27].

Earlier studies [9, 13, 32, 33] have examined roles of differential osmotic stress ($\Delta\pi$) and electrochemical stress (A–R) on the swelling behavior of expansive clays. Results of these studies illustrate how flow of solutes in the inter-layer space of expansive clays can alter $\Delta\pi$ and (A–R) and in turn the swelling properties. In comparison, kaolinites do not develop inter-layer swell as entry of water and solutes into their inter-layer space is prohibited by the strong inter-layer bonding [27]. The consequent weak inter-particle repulsion developed on external surfaces allows kaolinite particles to adopt flocculated structure in dilute (water content −1000 %) and concentrated (water content −40 to 50 %) suspensions [31, 36].

Guided by relevance of physico-chemical stresses in the geotechnical response of inactive clays that are deposited in marine environments, this paper examines the relative influence of differential osmotic stress and electrochemical stress on the consolidation behavior of kaolinites subjected to slurry consolidation in 500 and 9649 mg/L sodium ion

✉ Sudhakar Rao
msrao@civil.iisc.ernet.in

[1] Indian Institute of Science, Bengaluru, India

solutions. Synthetic seawater [6] is contributed by 9649 mg/L of sodium ions, which formed the basis of choosing it as one of the ion concentration. The other (500 ppm sodium) solution was selected to highlight influence of variations in electrolyte concentration.

The differential osmotic stress and electrochemical stress operative in kaolinite specimens at various consolidation pressures are calculated from equations described in Sects. 2.1, 2.2, and 2.3. Inputs to equations are obtained by measuring (a) dissolved salt concentrations in pore water and consolidometer reservoir water at each consolidation pressure (b) void ratio/water content of kaolinite specimen at each consolidation pressure, (c) specific surface area and (d) cation exchange capacity of kaolinite.

2 Theoretical considerations

2.1 Equivalent net stress from osmotic suction

Rao and Thyagaraj [32] have indicated that osmotic flow of salt solution from external reservoir to pore water of the clay induces an additional equivalent net stress component (p_π):

$$p_\pi = \alpha\Delta\pi = \alpha\left(\pi_{1f} - \pi_{2f}\right) \tag{2}$$

In Eq. (2), osmotic efficiency (α) varies between 0 and 1 and determines the magnitude of $\Delta\pi$ contribution to true mean effective stress. Values of $\alpha = 0$ and 1 imply imperfect and perfect semi-permeable membrane behavior, respectively. In Eq. (2), π_{1f} represents equilibrium osmotic suction in pore water of clay and π_{2f} represents equilibrium osmotic suction of the external (reservoir) solution.

When ions flow from external reservoir to pore water in response to differential osmotic stress, it induces an additional equivalent net stress (p_π) and enhances electrochemical stress (A–R).

2.2 Calculation of osmotic efficiency

The osmotic efficiency of the Na-amended kaolinites is calculated from the Fritz-Marine Membrane Model (FMMM) [16, 21, 25]. The model is based on the premise that at osmotic equilibrium, thermodynamic forces acting across the membrane are balanced by the sum of mechanical-frictional forces between ions and water/membrane. Anions attempting to migrate in the pore space are repelled by the negative mid-plane potential; the tendency to exclude anions also hinders cation migration because cations need anions to maintain electrical neutrality. Consequently, as the porosity of the clay decreases, increased overlap of diffuse ion layers enhances frictional resistance between anions and clay membrane that in turn enhances the osmotic efficiency of the clay. The model calculates osmotic efficiency from soil porosity, cation and anion concentrations in pore water, average solute concentration in pore water and external reservoir, and frictional coefficients of the ions with pore water and clay structure and is expressed as:

$$\alpha = 1 - \frac{K_S(R_w + 1)}{\left[\left(R_w\frac{\bar{C}_a}{\bar{C}_c} + 1\right) + R_{wm}\left(R_m\frac{\bar{C}_a}{\bar{C}_c} + 1\right)\right]n} \tag{3}$$

In Eq. (3), $K_s = C_a/C_s$, where C_a is the anion concentration in pore water (mol/cm^3) and C_s represents average solute concentration (mol/cm^3) of pore water + reservoir water. R_w represents the frictional resistance between solutes and pore water and equals 1.63 for the NaCl amended kaolinite specimens used in the study [17]. R_m represents the tendency of ions to be retarded by frictional resistance with membrane walls. Neglecting electrostatic effects, R_m is obtained by considering the hydrated radii of ions and ranges between 1.13 and 1.80 for NaCl–H_2O system [16, 21, 23, 24]. R_{wm} represents the friction of anions with both membrane (m) and pore water (w) and is >1 for compact clay ($n \ll 40$ %) and reduces with increasing porosity [21]. As porosity tends to zero, the contribution from R_{wm} can transform even, low to non-active clays, such as illite and kaolinite into ideal membranes (osmotic efficiency unity).

2.3 Electrochemical stress (A–R)

The attraction (A) stress between clay particles is a function of particle separation [27]:

$$A = \frac{C}{d_\mu^4}\ \text{dynes/cm}^2 \tag{4}$$

where d_α is half distance between two clay particles (μm) and C is a constant ranging from 0.6×10^{-3} to 1.6×10^{-3}; the average value of 1.1×10^{-3} is assumed for C in the present study. The value of d_μ is obtained as [40]:

$$d_\mu = \frac{100\ w}{S} \times 10^4 \tag{5}$$

where w is gravimetric water content (mass percent) and S is the surface area of kaolinite (m^2/g). The inter-particle repulsion pressure (R) between clay particles arises from overlap of diffuse ion layers and is obtained as [39, 40]:

$$R = 2n'kT(\cosh u' - 1) \tag{6}$$

where R represents the inter-particle repulsion pressure/swell pressure, n' is the ion concentration in pore water (mol/L), k is Boltzmann constant (1.38×10^{-16} ergs/K), T is absolute temperature (K) and u' is the mid-plane

potential between two parallel clay particles [20, 27, 39, 40]. The procedure for obtaining the mid-plane potential described by van Olphen [39] is adopted in the present study. The difference between A and R gives the electrochemical stress (A–R).

2.4 Incorporation of p_π in true effective stress

Mitchell and Soga [27] define true inter-granular stress as:

$$\sigma_1' - \sigma' = A - R \tag{7}$$

where, σ_1' is true inter-granular stress and is contributed by σ' (conventional effective stress) and electrochemical stress (A–R). The true inter-granular stress [11, 27] is given as:

$$\sigma' = \sigma - u \tag{8}$$

where σ is the total stress and u is the pore water pressure.

According to Fredlund et al. [15], the osmotic stress (p_π) is an independent, isotropic, stress state variable. The physico-chemical contributions to true effective stress (σ_1') are modified to incorporate p_π component (in addition to A–R); the true effective stress (σ_1') of Mitchell and Soga [27] becomes:

$$\sigma_1' = \sigma' + (A - R) + p_\pi \tag{9}$$

3 Materials and methods

Commercial kaolinite sieved through 425-micron sieve and oven dried at 105 °C was used in the study. 500 ppm (mg/L), and 9649 ppm sodium ion solutions were prepared using analytical-grade sodium chloride salt. The higher sodium ion concentration (9649 ppm) is representative of its concentration in substitute ocean water [6].

3.1 Index properties

Grain size distribution [3], specific gravity [8] liquid and plastic limits [5] of kaolinite were performed as per ASTM Standard procedures. The kaolinite specimen has specific gravity of 2.6, liquid limit of 48 %, plasticity index of 18 % and is composed of 12 % sand, 85 % silt and 3 % clay sized fractions (Table 1). The cation exchange capacity (CEC) of kaolinite was determined by extracting the exchangeable calcium, magnesium, sodium and potassium ions with neutral ammonium acetate solution [37]. The sum of displaced exchangeable ions gave the CEC of kaolinite (4.6 meq/100 g, Table 1). The surface area of kaolinite (10 m^2/g, Table 1) was measured by BET technique. The pH of kaolinite was measured based on ASTM procedure [7]; the pH of 1:1 (mass %) kaolinite—500 ppm Na suspension and kaolinite—9649 ppm Na suspension was measured and corresponded to 7.6 and 7.4, respectively. The point of zero charge (PZC) of kaolinite corresponds to 4.6 [2]. As pH of kaolinite suspensions (7.4–7.6) are larger than the PZC value (4.6), protons (H^+) are drawn away from surface hydroxyl groups into the solution and the negatively charged hydroxyl surface of kaolinite contributes to its CEC [34].

Table 1 Index and engineering properties of kaolinite

Parameter	Value
BET surface area (m^2/g)	10
Cation exchange capacity (meq/100 g)	4.6
Ca—3.5; Mg—0.3; K—0.2; Na—0.6	
Specific gravity	2.6
Liquid limit (mass %)	48
Plasticity index (mass %)	18
Particle size distribution (mass %)	
Sand fraction (4.75–0.075 mm)	12
Silt fraction (0.075–0.002 mm)	85
Clay fraction (<0.002 mm)	3

3.2 Slurry consolidation tests

Slurry consolidation (SC) specimens were prepared from kaolinite slurries mixed with 500 and 9649 ppm Na solutions at 97 % moisture content [representing twice the liquid limit water content (mass %)]. The 500 and 9649 ppm kaolinite slurries were prepared by manually mixing 61 g of kaolinite with 60 mL of the given sodium chloride solution for 30 min using a spatula. The homogenous slurry was stepwise poured in 60 mm diameter consolidation ring in three layers to total thickness of 30 mm; air entrapment was prevented by gently tapping the slurry with glass rod after pouring each layer. Pore water from 500 and 9649 ppm slurries were allowed to drain for 10 h (under self-weight) and for a further period of 1 h after placement of the top porous stone and loading pad into syringe. The consolidometer was assembled and placed in the loading frame. Pore water that had drained from the consolidation ring during self-weight consolidation of kaolinite slurry was poured back into the consolidometer reservoir, and the reservoir was topped up with ultra-pure water (electrical conductivity = 12 μS/cm). After 12 h (allowed for any swelling which was nil), the seating load of 6.25 kPa was applied and time-settlement readings were recorded for 24 h. After 24 h consolidation at 6.25 kPa, the consolidometer was dismantled and the 6.25 kPa SC (slurry consolidated) specimen was used for pore water extraction. Similarly, SC specimens were prepared at consolidation pressures of 25, 100, 200 and 400 kPa using 500 and 9649 ppm kaolinite slurries. In each

slurry series (500/9649 ppm slurry), four separate specimens were incrementally loaded (load increment ratio = unity) to consolidation pressures of 25, 100, 200 and 400 kPa, respectively. Each incremental load was maintained for 24 h though time-settlement plots indicated that kaolinite specimens achieved 90 % consolidation in <1 min (Fig. 1a, b). After attaining desired consolidation pressure (25/100/200/400 kPa), the four specimens were stepwise unloaded to 6.25 kPa and then dismantled. Each load was removed at 1 h intervals. Thus, total of 10 SC specimens are produced; five specimens being produced at each Na^+ ion concentration. The 400 kPa specimen was incrementally loaded from 6.25 to 400 kPa in 7 days (includes 1 day at 6.25 kPa) and was dismantled in 6 h after stepwise unloading to 6.25 kPa (includes 1 h at 6.25 kPa). Likewise, the 25 kPa specimen was incrementally loaded from 6.25 to 25 kPa in 3 days and dismantled in 2 h after stepwise unloading to 6.25 kPa. The 100 kPa specimen was incrementally loaded from 6.25 to 100 kPa in 5 days and dismantled in 4 h after stepwise unloading to 6.25 kPa. The 200 kPa specimen was incrementally loaded from 6.25 to 200 kPa in 6 days and dismantled in 5 h after stepwise unloading to 6.25 kPa. Thus, the pore solution remained in contact with consolidometer reservoir solution between 7 days 6 h (400 kPa specimen) to 1 day (6.25 kPa specimen).

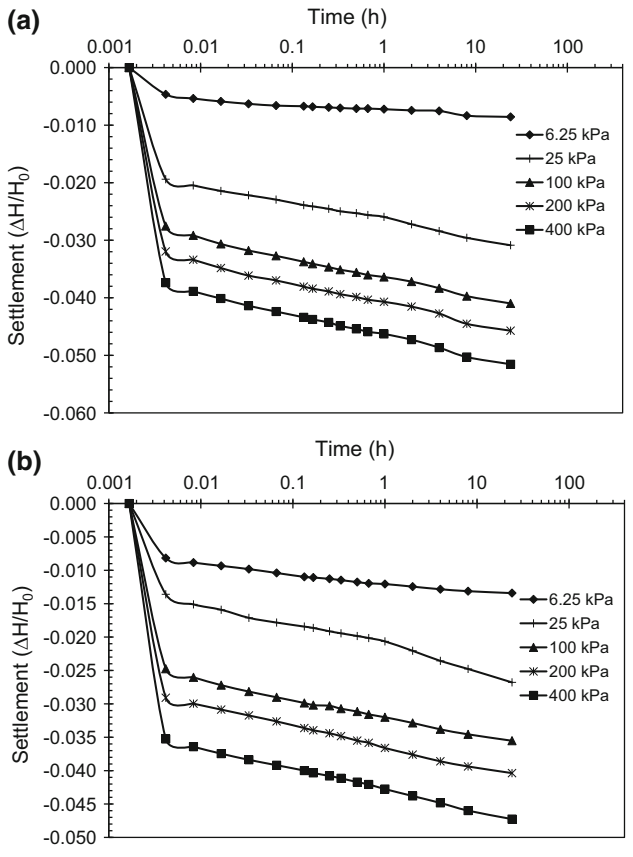

Fig. 1 **a** Time-settlement behavior of 500 ppm specimens at different consolidation pressures. **b** Time-settlement behavior of 9649 ppm specimens at different consolidation pressures

After completion of unloading sequence, water was siphoned from the consolidometer reservoirs into sealed containers and the consolidometers were dismantled. The ASTM pore water squeezing method [4] extracted the pore water of the unloaded specimens. The clay specimen scooped from the dismantled consolidometer ring was hand-packed into extraction mold and squeezed in static press until 12–15 mL of pore water collected in 30-mL vial. The extracted pore water and siphoned consolidometer reservoir water of each consolidation pressure specimen were analyzed for cation (sodium, calcium, magnesium, potassium) and anion (chloride, bicarbonate, sulfate) concentrations. The sodium, calcium, magnesium and potassium ion concentrations were measured using inductively coupled plasma optical emission spectrometer (ICPOES) (model: Thermo-ICAP 6500). The chloride and sulfate ion concentrations were determined using ion chromatography system (Dionex ICS 2000) configured with hydroxyl-based anion retention column. The bicarbonate ion concentration was determined using automatic titrator (Metrohm 877 Titrino Plus).

Separate experiments were performed to examine the influence of long-duration loading on changes in pore solution composition of kaolinite specimens prepared with 9649 ppm Na solution. After stepwise loading to 25 kPa in 3 days, the specimen was maintained at same vertical effective stress (25 kPa) for 53 additional days. After 56 days, the specimen was dismantled in 2 h upon stepwise unloading to 6.25 kPa. Likewise, after attaining the consolidation pressure of 100 kPa in 5 days, the specimen was maintained at the same vertical effective stress (100 kPa) for an additional period of 53 days. After 58 days, the specimen was dismantled in 4 h after stepwise unloading to 6.25 kPa. The pore solution compositions of the specimens after dismantling from consolidometers were determined by the earlier described procedure.

3.3 Measurement of swell potential

Kaolinite slurries prepared with 500 and 9649 ppm Na solutions were consolidated to 400 kPa and unloaded to 6.25 kPa by the procedure described in Sect. 3.2. After unloading to 6.25 kPa, the saline water in the oedometer reservoirs of the 500 and 9649 ppm kaolinite specimens was replaced with ultra-pure water; changes in dial gage reading were periodically monitored for 7 days to record possible osmotic swell of specimens from dilution of the saline pore water (1397 and 23,120 mg/L) by the intruded ultra-pure water [38].

To examine possibility of specimen compression at larger vertical stresses from dilution of pore solution, kaolinite slurry prepared with 9649 ppm Na solution was stepwise consolidated (duration of each load 24 h) to 100 kPa. After 24 h of consolidation at 100 kPa, the saline water in the consolidometer reservoir was replaced with ultra-pure water and dial gage reading were monitored for 7 additional days for possible compression strains.

4 Results and discussion

4.1 Ion concentrations in pore water

The cation and anion concentrations in pore water of the 500 and 9649 ppm specimens at each consolidation pressure are listed in Tables 2 and 3. The ion composition of pore water dominate in sodium and chloride ions with minor presence of calcium, magnesium, potassium, bicarbonate and sulfate ions (Tables 2, 3). Remolding kaolinite with sodium chloride solutions results in the dominant presence of sodium and chloride ions in pore water. The minor ions (calcium, magnesium, potassium, bicarbonate and sulfate) in the pore water are contributed by the dissolved salts of natural kaolinite plus contaminants present in the added sodium chloride solution. The 6.25 kPa specimens, 25 kPa specimens, 100 kPa specimens, 200 kPa specimens and 400 kPa specimens were in contact with the reservoir water for periods of 1, 3, 5, 6 and 7 days, respectively, during the consolidation process. Sodium and chloride ion concentrations in pore water of the 500 ppm specimens are lower than their respective initial concentrations by 10–11 and 17–27 % at all consolidation pressures (Table 2). Likewise, sodium and chloride ion concentrations in the pore water of the 9649 ppm specimens are lower than their respective initial concentrations by 11–24 and 11–22 % at all consolidation pressures (Table 3). Reductions in sodium and chloride ion concentrations in pore water of both specimens are larger than experimental error of ±3 %. In comparison, changes in minor ion concentrations in pore water (in comparison with respective initial concentrations) at various consolidation pressures are larger than the experimental error (±3 %). Pattern of results in Tables 2 and 3 indicate that sodium and chloride ions mainly diffuse from pore water to reservoir water from the chemical and hydraulic boundaries (illustration in Fig. 2). Ion composition data in Tables 2 and 3 are expressed in terms of molarity for calculating osmotic efficiency and osmotic pressures latter (Table 4).

Figure 3 plots variations in sodium and chloride ion concentrations in pore water of 25 and 100 kPa specimens upon prolonged loading. Sodium and chloride concentrations in pore water of both specimens experience 15–17 % reductions (from respective initial concentrations) after 3 and 5 days of consolidation (under 25 and 100 kPa). Increasing the consolidation duration from 3 to 56 days reduces the sodium and chloride ion concentrations in pore water of the 25 kPa specimens by 18–19 % (with reference to 3 day concentrations). Increasing the consolidation duration from 5 to 58 days causes smaller reduction (7–9 %) in sodium and chloride ion concentrations in pore water of the 100 kPa specimens (with reference to 5 day concentrations). Kaolinite specimens undergo rapid primary consolidation (less than 1 min) and gradual secondary compression (up to 58 days, Fig. 1a, b). Expulsion of pore water and dissolved salts from soil pores under transient hydraulic gradients (from applied vertical stress) is therefore complete in <1 min. External migration of sodium and chloride ions during subsequent creep is driven by chemical concentration gradients and occurs as the kaolinite membrane functions as non-ideal osmotic membrane. The non-ideal behavior of clay membrane would also allow the expelled dissolved salts to re-enter clay pores along within flowing water molecules from oedometer reservoir (to dilute pore solution). Additionally, the volume of osmotic induced flow of water molecules into clay pores are restricted by volume of kaolinite voids (V_V) permitted for the specimen by consolidation pressure and initial soil conditions (water content, void ratio).

Table 2 Pore water composition of 500 ppm specimens at different consolidation pressures

Consolidation pressure, σ_1' (kPa)	Cations (mg/L)				Anions (mg/L)		
	Calcium	Potassium	Magnesium	Sodium	Bicarbonate	Sulfate	Chloride
0.001	178	20	13	508	59	11	880
6.25	220	22	14	426	76	21	729
25	195	19	14	406	102	12	670
100	230	28	18	455	107	17	702
200	193	46	14	428	50	18	728
400	197	22	14	403	106	11	644

Table 3 Pore water composition of 9649 ppm specimens at different consolidation pressures

Consolidation pressure, σ'_1 (kPa)	Cations (mg/L)				Anions (mg/L)		
	Calcium	Potassium	Magnesium	Sodium	Bicarbonate	Sulfate	Chloride
0.001	699	50	37	10,324	38	333	15,400
6.25	699	55	39	9144	40	330	13,738
25	670	54	37	8778	203	346	13,145
100	672	49	38	8589	38	304	12,984
200	606	49	35	7898	41	320	12,002
400	672	52	37	8654	99	357	13,248

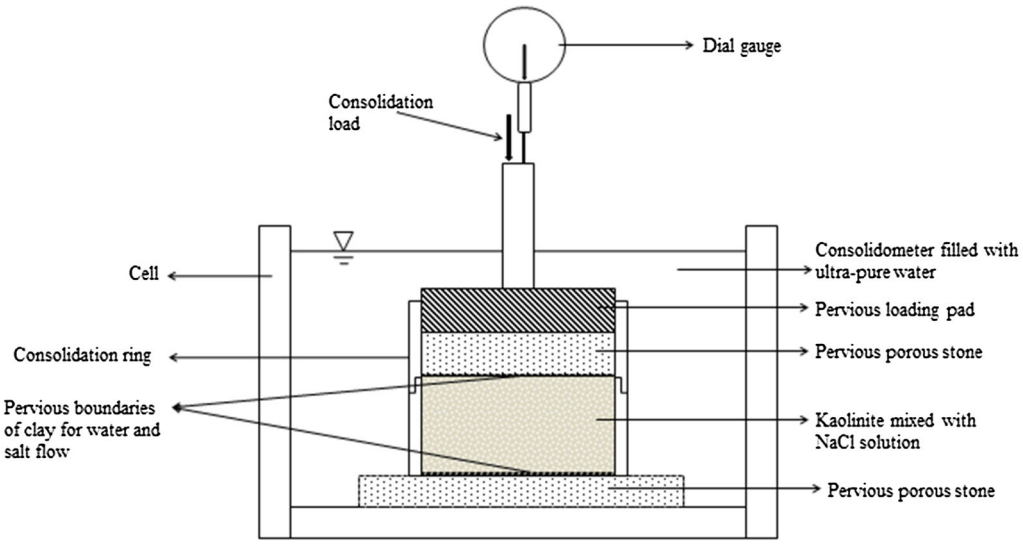

Fig. 2 Schematic diagram of consolidometer showing pervious boundaries for water and ion flow

Table 4 Osmotic efficiency computation of 9649 and 500 ppm specimens at different consolidation pressures

Consolidation pressure (kPa)	n (porosity)	C_a (mol/cm^3)	C_c (mol/cm^3)	C_s (mol/cm^3)	R_w	R_m	R_{wm}	α
9649 ppm series								
6.25	0.591	0.00,038	0.000397	0.000515	1.63	1.8	0.27	0.0049
25	0.569	0.00037	0.00038	0.000513	1.63	1.8	0.28	0.0061
100	0.537	0.000366	0.000373	0.0005095	1.63	1.8	0.34	0.0062
200	0.514	0.0003385	0.000343	0.0004945	1.63	1.8	0.34	0.015
400	0.484	0.000374	0.000376	0.0005215	1.63	1.8	0.48	0.0153
500 ppm series								
6.25	0.567	0.00002	0.0000185	0.0000305	1.63	1.8	0.1	0.005
25	0.539	0.0000189	0.0000176	0.0000305	1.63	1.8	0.1	0.0069
100	0.5	0.00001979	0.00001977	0.000036	1.63	1.8	0.1	0.044
200	0.474	0.0000205	0.0000186	0.0000395	1.63	1.8	0.1	0.103
400	0.439	0.0000181	0.0000175	0.000033	1.63	1.8	0.4	0.1437

Chemical equilibrium in solutions separated by non-ideal membrane, under restrained volumetric strain conditions is difficult to establish. Sodium and chloride ion concentrations attained in pore water and consolidometer reservoir water at end of given duration reflects transient ionic equilibrium condition of that load.

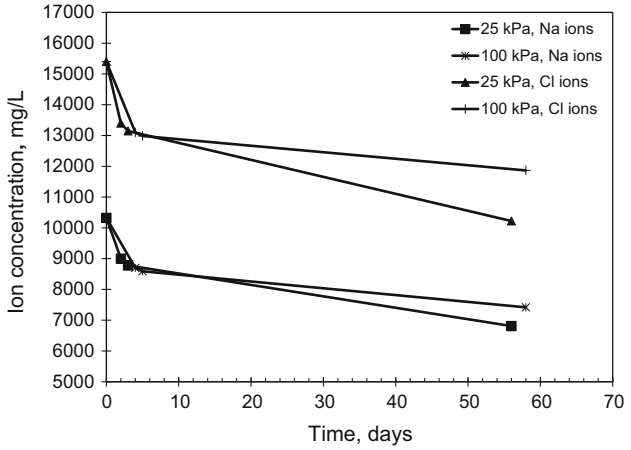

Fig. 3 Variations in sodium and chloride ion concentrations in pore water of 9649 ppm specimens subjected to prolonged loading

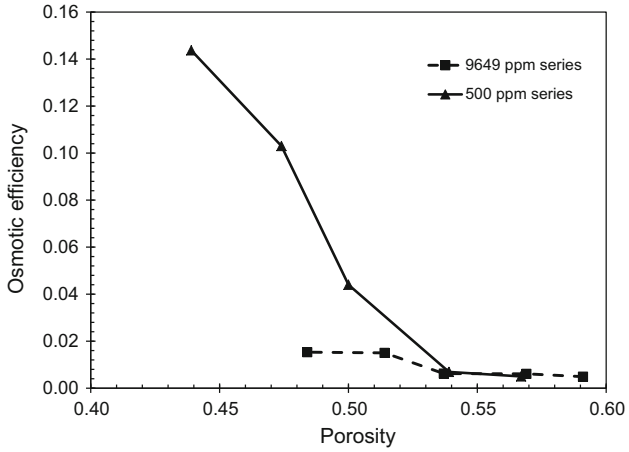

Fig. 4 Variation of osmotic efficiency with porosity for 500 and 9649 ppm specimens

4.2 Calculation of osmotic efficiency

Table 4 presents the osmotic efficiency calculated from the Marine and Fritz [16] Eq. (3) for the 9649 and 500 ppm specimens at different consolidation pressures. R_w represents the frictional resistance between ions (cations and anions) and pore water and is assigned value of 1.63 for the NaCl amended kaolinite specimens based on Fritz [16]. R_m represents the friction of anions and cation with clay (membrane) structure and is assigned value of 1.8 based on Fritz [16]. R_{wm} term represents the frictional resistance of anions with both membrane and pore water and is strong function of porosity. At given porosity (n), the least R_{wm} that yielded positive α (all other parameters remaining constant) defined the R_{wm} of the specimen at given consolidation pressure (Table 4). The porosity (n) values were obtained from experimental void ratios at different consolidation pressures (Table 4). C_a and C_c represent experimental chloride and sodium ion concentrations in pore water (mol/cm^3) at given consolidation pressure, while C_s represents the average of $M_{1f} + M_{2f}$ (mol/cm^3) at each consolidation pressure (Table 4). Inserting the appropriate values gave the osmotic efficiency of the 9649 and 500 ppm specimens at different consolidation pressures (Table 4). The osmotic efficiencies of 9649 ppm specimens (Table 4) range between 0.0049 and 0.0153 ($n = 0.591$–0.484) and between 0.005 and 0.1437 in case of the 500 ppm specimens ($n = 0.567$–0.439). The osmotic efficiencies of 9649 and 500 ppm series specimens increase with reduction in porosity (Fig. 4) apparently from increased interference to chloride migration into pores by the kaolinite micro-structure. Further, the 500 ppm specimen exhibits larger α than the 9649 ppm specimen at given porosity (Fig. 4) possibly as the larger diffuse ion layer thickness (21.55–22.9 Å, Table 5) associated with these clay particles retard the passage of chloride ions into the pore space more effectively (diffuse ion layer thickness of 9649 ppm specimens range between 4.8 and 5.17 Å, Table 5). The diffuse ion layer thickness ($1/\kappa$) of the 500 and 9649 ppm specimens at given consolidation pressure is obtained from the equation [27]:

$$\frac{1}{\kappa} = \sqrt{\left(\frac{\varepsilon kT}{8\pi n' e'^2 \nu'^2}\right)} \tag{10}$$

where ε is the dielectric constant of medium (water = 80), k is the Boltzmann's constant (1.38×10^{-16} erg/K), T is temperature in K (290 K), n' is sodium ion concentration in pore water at given consolidation pressure (Tables 2, 3), e' is elementary charge (4.77×10^{-19} esu), and ν' is sodium ion valence (unity).

4.3 Calculation of p_π

The contribution of p_π to true effective stress (σ'_1) at various consolidation pressures are presented in Table 7. The osmotic suctions of pore water (π_{1f}) and consolidometer reservoir water (π_{2f}) at different consolidation pressures are calculated from equations:

$$\pi_{1f} = M_{1f} R' T \tag{11a}$$

$$\pi_{2f} = M_{2f} R' T \tag{11b}$$

where M_{1f} and M_{2f} (mol/L) represent the dissolved salt concentration in pore water and consolidometer reservoir water after 24-h consolidation at given pressure and R′ and T have been defined previously in Eq. (1). The differential osmotic stress [$\Delta\pi = (\pi_{1f} - \pi_{2f})$] ranges from 1038 to 1446 kPa for 9649 specimens and from 37 to 82 kPa for 500 ppm specimens (Table 6); multiplication of the differential osmotic stress with corresponding osmotic

Table 5 Electrochemical stress of 9649 and 500 ppm specimens at different consolidation pressures

Consolidation pressure (kPa)	e	$2d$ (Å)	$1/\kappa$ (Å)	A (kPa)	R (kPa)	A–R (kPa)
9649 ppm series						
6.25	1.45	898	4.80	0.027	0	0.027
25	1.32	882	4.90	0.029	0	0.029
100	1.16	838	4.96	0.036	0	0.036
200	1.06	822	5.17	0.039	0	0.039
400	0.94	776	4.94	0.049	0	0.049
500 ppm series						
6.25	1.31	954	22.27	0.021	0	0.021
25	1.17	894	22.84	0.028	0	0.028
100	1.00	878	21.55	0.030	0	0.030
200	0.90	824	22.21	0.038	0	0.038
400	0.785	814	22.90	0.040	0	0.040

Table 6 $p\pi$ calculations for 9649 and 500 ppm specimens at different consolidation pressures

Consolidation pressure (kPa)	M_{1f} (mol/L)	M_{2f} (mol/L)	π_{1f} (kPa)	π_{2f} (kPa)	$\pi_{1f} - \pi_{2f}$ (kPa)	p_π (kPa)
9649 ppm series						
6.25	0.810	0.219	2008	542	1466	7.31
25	0.779	0.246	1932	611	1321	8.06
100	0.763	0.256	1892	635	1257	7.79
200	0.704	0.285	1745	707	1038	15.58
400	0.775	0.268	1922	663	1258	19.25
500 ppm series						
6.25	0.047	0.014	117	35	82	0.41
25	0.044	0.017	110	43	67	0.46
100	0.049	0.023	121	57	64	2.80
200	0.047	0.032	116	79	37	3.80
400	0.044	0.022	108	54	54	7.77

efficiency give p_π that ranges between 7 and 19 kPa for the 9649 ppm specimens and from 0.41 to 7.77 kPa for 500 ppm specimens (Table 6). The larger p_π values of the 9649 specimens are consequence of larger $\Delta\pi$ values (Table 6).

4.4 Calculation of electrochemical stress (*A–R*)

The attraction and repulsion stresses operative in the 500 and 9649 ppm series specimens at different consolidation pressures were obtained from Eqs. (4) and (6). The half distance between particles (d) is calculated from Eq. (5). The attraction stress of the 500 ppm specimens ranges from 0.021 to 0.04 kPa and from 0.027 to 0.049 kPa for the 9649 ppm specimens (Table 5).

Calculations from Eq. (6) reveal that the 9649 and 500 ppm series specimens are devoid of inter-particle repulsion. Table 5 provides the experimental void ratio, calculated inter-particle separation (2d spacing), diffuse ion layer thickness, attraction and repulsion stress at each consolidation pressure. The thickness of diffuse ion layers mobilized on the kaolinite particle surfaces are far smaller than the 2d separations; consequently, overlap of diffuse ion layers and development of repulsion pressure at the experimental void ratios does not occur. Results of the consolidometer swell potential tests also validate their non-swelling nature as the 500 and 9649 ppm kaolinite specimens develop negligible osmotic swell potentials of 0.06–0.12 % at 6.25 kPa (Fig. 5). The 500 and 9649 ppm specimens experience larger swell potentials of 3.5 % from "mechanical swelling" on unloading the specimens from 400 to 6.25 kPa (Fig. 6). Upon replacement of saline water in consolidometers reservoir with ultra-pure water after elapse of 24 h loading at 100 kPa, the consolidated

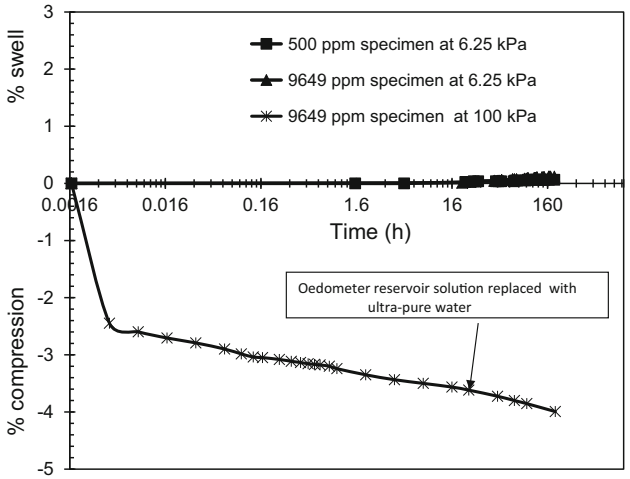

Fig. 5 % Swell, compression behavior of 500 and 9649 ppm specimens with time

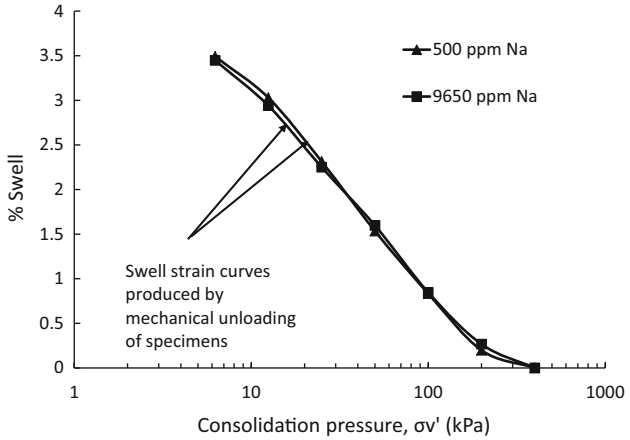

Fig. 6 % Swell of 500 and 9649 ppm specimens upon mechanical unloading

specimen experiences additional creep deformation of −0.38 % over next 7 days (Fig. 5).

4.5 Void ratio: true effective stress plots

Figure 7 compares void ratio—true effective stress (σ_1') plots of 500 and 9649 ppm specimens. The 9649 ppm specimens are less compressible than the 500 ppm specimens and exhibit larger void ratio at given true effective stress (Fig. 7). The 9649 and 500 ppm series specimens are subjected to similar effective vertical stress (σ_v': 6.25–400 kPa) during consolidation; however, of the two physico-chemical components, only p_π finitely contributes to true effective stress (Table 7). Further, the availability of higher p_π contribution (Table 7) enables the 9649 kaolinite specimens to sustain larger void ratio during consolidation (Fig. 7; Table 7).

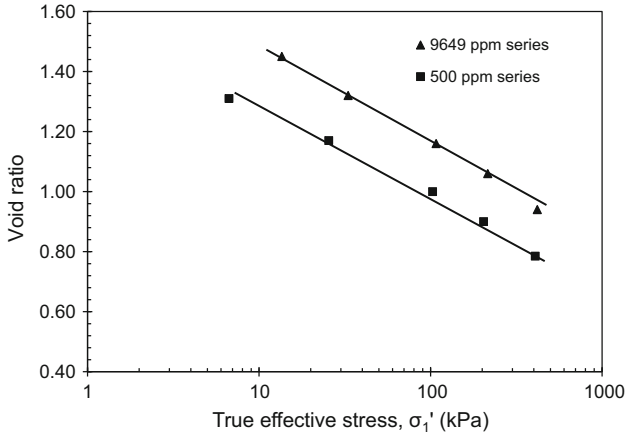

Fig. 7 Void ratio—σ_1' variations for 9649 and 500 ppm specimens

Table 7 True mean effective stress of 9649 and 500 ppm specimens at different consolidation pressures

σ_v' (kPa)	p_π (kPa)	A–R (kPa)	σ_1' (kPa)	e
9649 ppm series				
6.25	7.31	0.027	13.6	1.45
25	8.06	0.029	33.1	1.32
100	7.79	0.036	107.8	1.16
200	15.58	0.039	215.6	1.06
400	19.25	0.049	419.3	0.94
500 ppm series				
6.25	0.41	0.021	6.7	1.31
25	0.46	0.028	25.5	1.17
100	2.8	0.03	102.8	1
200	3.8	0.038	203.8	0.9
400	7.77	0.04	407.8	0.785

5 Conclusions

The true mean effective stress (σ_1') is mainly contributed by the physico-chemical component of p_π and conventional mean effective stress (σ_v'). Since kaolinite functioned as non-ideal osmotic membrane, the pore water of 9649 and 500 ppm specimens experienced 10–27 % reduction in sodium and chloride ion concentrations from migration of these ions under chemical and hydraulic gradients. The concentrations of sodium and chloride ions attained in pore water and consolidometer reservoir water at particular load application reflected transient ionic equilibrium condition. The osmotic efficiencies (α) were obtained using the Fritz-Marine Membrane Model.

The α values ranged between 0.27 and 0.48 and between 0.1 and 0.4 for the 9649 and 500 ppm specimens, respectively. The osmotic efficiency increased with reduction in porosity apparently from increased interference toward

migration of anions (chloride) into kaolinite micro-structure. The 500 ppm specimen exhibited larger α than the 9649 ppm specimen at given porosity possibly as the larger diffuse ion layer thickness (21.55–22.9 Å) retarded the passage of chloride ions into the pore space more effectively. Larger p_π values of the 9649 specimens (7–19 kPa) resulted from higher differential osmotic stress (π_{1f}–π_{2f}) component. The 500 and 9649 ppm specimens were contributed by marginal attraction stress (<0.05 kPa). Further, the inability of diffuse ion layers to overlap due to large inter-particle separations resulted in the absence of repulsion between kaolinite particles. Consequently, of the two physico-chemical components, only the p_π component finitely contributed to true mean effective stress. The availability of higher p_π contribution facilitated the 9649 ppm series specimens to sustain larger void ratio during consolidation in comparison with the 500 ppm series specimens.

References

1. Andersson-Sköld Y, Torrance JK, Lind B, Odèn K, Stevens RL, Rankka K (2005) Quick clay—a case study of chemical perspective in southwest Sweden. Eng Geol 82:107–118
2. Appelo CAJ, Postma D (1994) Geochemistry, ground water and pollution. CRC Press, Boca Raton
3. ASTM (2007a) Standard test method for particle-size analysis of soils. ASTM standard D422. American Society of Testing Materials (ASTM), Philadelphia PA
4. ASTM (2007b) Standard test method for pore water extraction and determination of the soluble salt content of soils by refractometer. ASTM standard D4542. American Society of Testing Materials (ASTM), Philadelphia PA
5. ASTM (2010) Standard test methods for liquid limit, plastic limit, and plasticity index of soils. ASTM standard D4318. American Society of Testing Materials (ASTM), Philadelphia PA
6. ASTM (2013) Standard practice for the preparation of substitute ocean water. ASTM standard D1141. American Society of Testing Materials (ASTM), Philadelphia PA
7. ASTM (2013) Standard test method for pH of soils. ASTM standard D4972. American Society of Testing Materials (ASTM), Philadelphia PA
8. ASTM (2014) Standard test methods for specific gravity of soil solids by water pycnometer. ASTM standard D854. American Society of Testing Materials (ASTM), Philadelphia PA
9. Barbour SL, Fredlund DG (1989) Mechanics of osmotic flow and volume change in clay soils. Can Geotech J 26:551–562
10. Bjerrum L, Loken T, Heiberg S, Foster R (1969) A field study of factors responsible for quick clay slides. In: Proceedings of the 7th international conference on soil mechanics and foundation engineering, Mexico City, 2:531–540
11. Budhu M (2007) Soil mechanics and foundations. Wiley, New York
12. Carretero S, Rapaglia J, Bokuniewicz H, Kruse E (2013) Impact of sea-level rise on salt water intrusion length into the coastal aquifer, Partido de La Costa, Argentina. Cont Shelf Res 61–62:62–70
13. Maio Di (1996) Exposure of bentonite to salt solution: osmotic and mechanical effects. Geotechnique 46:695–707
14. Eilertsen SR, Hansen L, Bargel HT, Solberg I-L (2008) Clay slides in the Malselv valley, northern Norway: characteristics, occurrence, and triggering mechanism. Geomorph 93:548–562
15. Fredlund DG, Rahardjo H, Fredlund MD (2012) Unsaturated soil mechanics in engineering practice. Wiley, NY
16. Fritz SJ (1986) Ideality of clay membranes in osmotic process: a review. Clay Clay Miner 34:214–223
17. Fritz SJ, Marine IW (1983) Experimental support for a predictive osmotic model of clay membranes. Geochim Cosmochim Ac 47:1515–1522
18. Gadd NR (1962) Surficial geology of the Ottawa area. Geological Survey of Canada, paper 62-16
19. Gylland A, Long M, Emdal A, Sandven R (2013) Characterisation and engineering properties of Tiller clay. Eng Geol 164:86–100
20. Karnlan O (1997) Bentonite swelling pressure in strong NaCl solutions. Correlations between model calculations and experimental data. SKB technical report 97-31
21. Keijzer ThJS (2000) Chemical osmosis in natural clayey materials. Geologica Ultraiectina 196. Ph. D. thesis, Utrecht University
22. Kerr PF (1979) Quick clay and other slide forming clays. Eng Geol 14:173–181
23. Kharaka YK, Berry FAF (1973) Simultaneous flows of water and solutes through geological membranes: I. Experimental INVESTIGATION. Geochim Cosmochim Ac 37:2577–2603
24. Marcus Y (1997) Ion properties. Marcel Dekker, New York
25. Marine IW, Fritz SJ (1981) Osmotic model to explain anomalous hydraulic heads. Water Resour Res 17:73–82
26. Melloul AJ, Goldenberg LC (1997) Monitoring of Seawater intrusion in coastal aquifers: basics and local concerns. J Environ Manag 51:73–86
27. Mitchell JK, Soga K (2005) Fundamentals of soil behavior, 3rd edn. Wiley, Hoboken
28. Ohtsubo M, Higashi T, Kanayama M (2007) Depositional geochemistry and geotechnical properties of marine clays in the Ariake bay area Japan. In: Tan TS et al (eds) Characterisation and engineering properties of natural soils, vol 3. Talor & Francis, Milton Park, pp 1893–1938
29. Pulido-Leboeuf P (2004) Seawater intrusion and associated processes in a small coastal complex aquifer (Castell de Ferro, Spain). Appl Geochem 19:1517–1527
30. Rao SM, Shivananda P (2005) Role of curing temperature in progress of lime-soil reactions. Geot Geol Eng 23:79–85
31. Rao SM, Sridharan A (1985) Mechanisms controlling volume change behaviour of kaolinite. Clay Clay miner 34:323–328
32. Rao SM, Thyagaraj T (2007) Swell compression behavior of compacted clays under chemical gradients. Can Geotech J 44(5):520–532
33. Rao SM, Thyagaraj T, Thomas HR (2006) Swelling of compacted clay under osmotic gradients. Geotechnique 56(10):707–713
34. Ryan PC (2014) Cation exchange capacity of tropical soil clays as a function of time and precipitation. 2014 GSA annual meeting, Vancouver, British Columbia
35. Solberg I-L (2003) Geological development and stability along the Mortenelva river in the Malselv valley, Troms. Diploma thesis, Department of Geology and Mineral Resources Engineering, Faculty of Engineering Science and Technology, NTNU, Trondheim (**in Norwegian**)
36. Sridharan A, Rao SM, Murthy NS (1985) Free swell index of soils: a need for re-definition. Indian Geotech J 15:94–95
37. Sumner ME, Miller WP (1996) Cation exchange capacity, and exchange coefficients. In: Sparks DL (ed) Methods of soil analysis. Part 2: chemical properties (3rd edn). ASA, SSSA, CSSA, Madison, WI

38. Thyagaraj T, Rao SM (2013) Osmotic swelling and osmotic consolidation behavior of compacted expansive clay. Geotech Geol Eng 31:435–445
39. Van Olphen H (1963) Clay colloid chemistry. Wiley, London
40. Yong RN, Warkentin BP (1975) Soil properties and behavior. Elsevier, Amsterdam
41. Zghibi A, Tarhouni J, Zouhri L (2013) Assessment of sea water intrusion and nitrate contamination on the ground water quality in the Korba costal plain of Cap-Bon, North- east of Tunisia. J Afr Earth Sci 87:1–12